Journal of Solid State Chemistry 182 (2009) 496–501

Contents lists available at ScienceDirect

Journal of Solid State Chemistry

journal homepage: www.elsevier.com/locate/jssc

Superstructure of a phosphor material $Ba_3MgSi_2O_8$ determined by neutron diffraction data

Cheol-Hee Park [a,*], Seung-Tae Hong [a], Douglas A. Keszler [b]

[a] LG Chem Research Park, Daejeon 305-380, South Korea
[b] Department of Chemistry, 153 Gilbert Hall, Oregon State University, Corvallis, OR 97331-4003, USA

ARTICLE INFO

Article history:
Received 14 October 2008
Received in revised form
20 November 2008
Accepted 20 November 2008
Available online 3 December 2008

Keywords:
Barium magnesium silicate
$Ba_3MgSi_2O_8$
Phosphor
Crystal structure
Superstructure
Neutron diffraction data

ABSTRACT

$Ba_3MgSi_2O_8$, a phosphor host examined for use in white-light devices and plant-growth lamps, was synthesized at 1225 °C in air. Its crystal structure has been determined and refined by a combined powder X-ray and neutron Rietveld method ($P\bar{3}$, $Z=3$, $a=9.72411(3)$ Å, $c=7.27647(3)$ Å, $V=595.870(5)$ Å^3; $R_p/R_{wp}=3.79\%/5.03\%$, $\chi^2=4.20$). Superstructure reflections, observed only in the neutron diffraction data, provided the means to establish the true unit cell and a chemically reasonable structure. The structure contains three crystallographically distinct Ba atoms—Ba1 resides in a distorted octahedral site with S_6 ($\bar{3}$) symmetry, Ba2 in a nine-coordinate site with C_3 (3) symmetry, and Ba3 in a ten-coordinate site with C_1 (1) symmetry. The Mg atoms occupy distorted octahedral sites, and the Si atom occupies a distorted tetrahedral site.

1. Introduction

The silicate $Ba_3MgSi_2O_8$ has received recent attention because Eu- and Mn-doped powders have exhibited efficacy in white-light devices [1–4], supporting development of fluorescent and plant-growth lamps [5–7]. In addition, the narrow blue emission band of the Eu-doped material allows use for color correction purposes [5].

Considering that the luminescence properties have been understood and explained on the basis of a largely unresolved crystal structure [1,3–7], it is important to establish the correct atomic arrangement. Since the report by Klasens and co-workers in 1957 [7], $Ba_3MgSi_2O_8$ has been assumed to be isostructural to the mineral merwinite $Ca_3MgSi_2O_8$, which was initially assigned an orthorhombic structure [7]. Later, Moore and Araki revised the structure to a monoclinic type [8]. In this work, we have found that the structure of $Ba_3MgSi_2O_8$ is closely related to the monoclinic structure of merwinite, although it crystallizes in the trigonal system. Here, we describe the synthesis and the crystal structure of $Ba_3MgSi_2O_8$, where neutron powder diffraction data has played a crucial role in revealing a previously unidentified superstructure.

2. Experimental

Powder samples of $Ba_3MgSi_2O_8$ were prepared by solid-state reaction of stoichiometric mixtures of $BaCO_3$ (99.95%, Alfa), MgO (99.99%, High Purity Chemicals) and SiO_2 (99.99%, 1–3 mm pieces, Cerac.). Prior to use, the large pieces of SiO_2 were ground into fine powders in an alumina mortar and pestle. The SiO_2 powder was then mixed with the remaining reagents and ground as an ethanol paste (100%, Duksan) in a ball mill with zirconia balls for four days. After milling, the zirconia balls were removed, and the mixture was dried overnight at 120 °C. The mixture was then pressed into pellets and heated at 1225 °C for a total of three days with three intermediate grinding and pressing steps; the yield was approximately 96% by weight with minor impurities of Ba_2SiO_4 [9] and $BaMgSiO_4$ [10]. Inductively coupled plasma (ICP) analysis by using a Perkin-Elmer Optima 5300DV led to results consistent with the stated composition with trace amounts of Zr (0.085% by weight), which may be transferred during the extended milling with zirconia balls.

Powder X-ray diffraction (XRD) data were collected at room temperature on a Bragg-Brentano diffractometer (Bruker-AXS Advance D8) with a Cu X-ray tube, a focusing primary Ge (111) monochromator ($\lambda=1.5406$ Å), and a position sensitive Väntec detector with a 6° slit. Data acquisition covered the angular range $10^\circ \leqslant 2\theta \leqslant 151^\circ$ at a step width of 0.016671° and a total measurement time of 13 h.

* Corresponding author. Fax: +82 42 861 2057.
E-mail address: pmoka@lgchem.com (C.-H. Park).

0022-4596/$ - see front matter © 2008 Elsevier Inc. All rights reserved.
doi:10.1016/j.jssc.2008.11.024

Neutron powder diffraction data were collected at room temperature in air by using instrumentation at the Korea Atomic Energy Institute, Daejeon, Korea. The HANARO HRPD system is equipped with a 32-He-3 multi-detector and a Ge (331) monochromator. The data were collected with a wavelength of 1.8352 Å over the 2θ range of 10°–145° with a step of 0.05° and a total measurement time of 3 h. The sample size was approximately 8 g.

The structure determination and refinement were performed by using TOPAS software [11] and the indexing program TREOR90 [12].

3. Results and discussion

3.1. Synthesis

Several different synthesis strategies were used in attempts to produce single-phase material. Preparative temperatures were varied between 1100 and 1425 °C; heating times were adjusted from 12 to 216 h; and the effects of various fluxes, e.g., $LiBO_2$, Li_2CO_3, and Na_2CO_3, were examined. As evident from analysis of XRD patterns, the products always contained small amounts of Ba_2SiO_4 and $BaMgSiO_4$. Heating a mixture of Ba_2SiO_4 and $BaMgSiO_4$ in a 1:1 molar ratio also produced a similar product; heating off-stoichiometry mixtures of these two components simply increased the relative concentration of the major reagent in the product. It was also observed that long heating times at temperatures higher than 1295 °C led to increased amounts of impurities, suggesting that $Ba_3MgSi_2O_8$ is not stable above this temperature. It seems that the impurity phases have sufficient thermodynamic or kinetic stability to compete with the formation of $Ba_3MgSi_2O_8$ under the stated conditions. While the amounts of secondary phases vary according to the synthesis conditions, the crystal structure of $Ba_3MgSi_2O_8$ is fixed within the temperature range investigated; the sample used for collection of diffraction data and subsequent analysis was synthesized at 1225 °C for 3 days. In this sample, the weight percentages of the components were found from the Rietveld refinement (Supporting Information) to be 96% ($Ba_3MgSi_2O_8$), 3% (Ba_2SiO_4), and 1% ($BaMgSiO_4$).

Continued examination of the synthesis methods will likely lead to single-phase material, but our main interest was to determine and refine the crystal structure, and fortunately, the small amounts of impurity phases did not affect the structure determination.

3.2. Powder X-ray and neutron analysis

Following initial inspection, it was obvious that the XRD pattern for $Ba_3MgSi_2O_8$ did not match the orthorhombic cell previously reported [7] or the monoclinic cells related to $Ca_3MgSi_2O_8$ [8]. Thus, to determine the correct unit cell, 20–30 peak positions of the XRD pattern at low angles were first obtained by single peak profile fitting with the program TOPAS. At this step, the known impurity peaks were excluded from consideration. A hexagonal unit cell with $a_o = 5.6072$ and $c_o = 7.2656$ Å was readily obtained from 20 peaks by using TREO90. No systematic absence was observed. At this point, a search of the inorganic crystal structure database (ICSD) for compounds with similar atomic ratios and unit cell dimensions produced matches with several compounds—$K_3NaM_2O_8$ (M = S, Se, or Cr), $K_3V_3O_8$, $BaNaPO_4$, $BaAg_2MnV_2O_8$, and Ca_2SiO_4 [13]—all forming in the same crystal structure. The structure of $K_3NaS_2O_8$ ($P\bar{3}m1$, $Z = 1$, $a_o = 5.6801$ Å, $c_o = 7.309$ Å) was chosen as the starting model for $Ba_3MgSi_2O_8$, where K, Na, and S atoms were replaced with Ba, Mg, and Si atoms, respectively, resulting in good Rietveld profile fitting with $R_p/R_{wp} = 3.23\%/4.14\%$ for the XRD data. The refined atom parameters for the subcell are given in the Supporting Information. The atomic displacement parameter (ADP) for atom O1, however, was abnormally large, and the interatomic distance of Si–O1 was unusually short, suggesting the structural model was only approximate. The Si–O distance was 1.523 Å, which is much shorter than the expected values from the sum of ionic radii: d(Si–O) = 1.64 Å [14]. Following symmetry reduction to space group $P\bar{3}$, the unusual features persisted.

Neutron diffraction data were collected, which would be very helpful, especially when used as a combination with X-ray data, to determine and confirm the structure. The neutron scattering length for the O atom ($b_{c,O} = 5.803$) is higher than those for Si ($b_{c,O} = 4.149$), Mg ($b_{c,Mg} = 5.375$), and the much heavier Ba ($b_{c,Ba} = 5.07$), providing a means to accurately place this light atom. Careful examination of the neutron diffraction pattern readily revealed several extra peaks that could be indexed by a $\sqrt{3} \times \sqrt{3} \times 1$ supercell ($a = \sqrt{3}a_o$ and $c = c_o$) of the smaller subcell. The relationship between the two cells is shown in Fig. 1. The atomic positions for the supercell were calculated appropriately from those for the subcell. The space group for the supercell would be $P\bar{3}1m$ if the subcell were just transformed to the larger supercell without displacement of the atoms. But, it should be noted that an equivalent structural model can be built for the space group $P\bar{3}$, which is a subgroup of $P\bar{3}1m$, allowing refinement of positional parameters for the O, Si, and some Ba atoms.

Finally, a combined Rietveld refinement of the X-ray and neutron diffraction data was employed to complete the structure determination. Comparison of refinement results for the two possible space groups ($P\bar{3}$ and $P\bar{3}1m$) showed that $P\bar{3}$ is the correct space group for $Ba_3MgSi_2O_8$ in terms of a plausible ADP for O1, reasonable Si–O interatomic distances, and reduced residuals (from 4.91% to 3.78% of R_p). The refinement parameters were scale factors, background, unit-cell parameters, peak-profile coefficients, atomic coordinates, and isotropic thermal parameters. For the impurity phases, the atomic parameters were fixed—only the scale factors and peaks profile functions were refined. Before the impurity phases were included in the refinement, the residual factors were $R_p/R_{wp} = 3.38\%/4.45\%$ for X-ray data, 4.85%/6.36% for neutron data, and 4.08%/5.48% for the combined datasets with χ^2 of 5.0. Including all impurities, the final residuals were reduced to $R_p/R_{wp} = 3.15\%/4.07\%$ for X-ray data, 4.50%/5.92% for neutron data, and 3.78%/5.02% for combined sets with χ^2 of 4.2. It should be mentioned that, although the residual values were reduced by

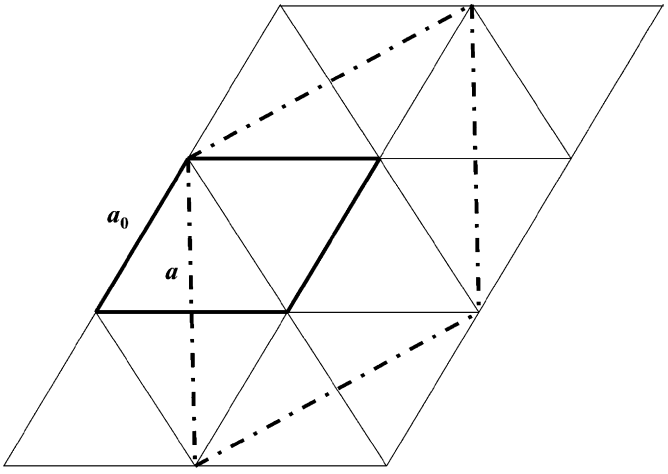

Fig. 1. Relationship between the subcell of a_o and the supercell of $a = \sqrt{3}a_o$ for $Ba_3MgSi_2O_8$. c-axis is not shown for clarity.

taking account of the impurities, they did not have any statistically meaningful effects on the refined parameters of the $Ba_3MgSi_2O_8$ structure; the main peaks for the secondary phases were relatively weak and did not overlap significantly with those from $Ba_3MgSi_2O_8$ (cf., Supporting Information.) The final profile fits are shown in Fig. 2, and powder refinement results are given in Table 1. The refined atomic and isotropic displacement parameters are given in Table 2, and the important bond distances and angles are listed in Table 3.

3.3. The structure

It is well known that many complex oxide structures can be related to the perovskite structure by considering variations on the stacking of layers of the type AX_3 and AX_2 as shown in Fig. 3 [15]. A represents large cations such as Ba^{2+} or Sr^{2+}, and X represents anions such as O^{2-} or a halide. The $Ba_3MgSi_2O_8$ structure can be described as a hexagonal layer stacking within the perovskite framework. Since the structural layout of the $\sqrt{3} \times$ $\sqrt{3} \times 1$ supercell for $Ba_3MgSi_2O_8$ is not much different from that of the subcell, consideration of the subcell is sufficient to provide a simple understanding; the subcell structure is illustrated in Fig. 4.

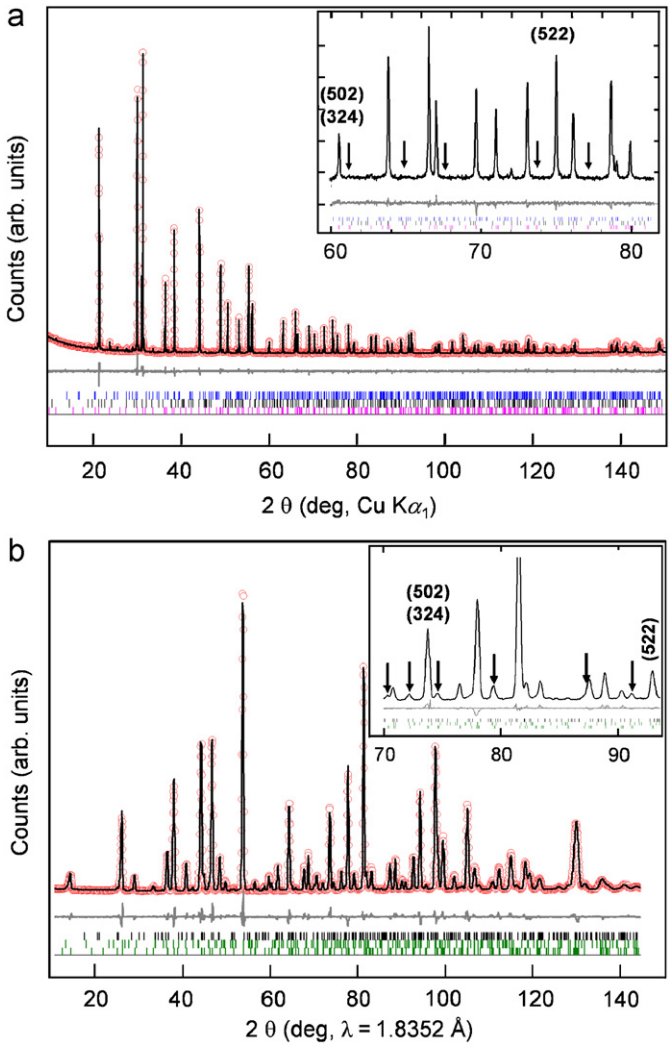

Fig. 2. Combined (a) X-ray ($\lambda = 1.5406$ Å) and (b) neutron ($\lambda = 1.8352$ Å) Rietveld refinement profiles for $Ba_3MgSi_2O_8$ recorded at room temperature. The circle line marks experimental points and the solid line is the calculated profile. The lower trace shows the difference curve, and the ticks denote expected peak positions for $Ba_3MgSi_2O_8$, $BaMgSiO_4$ and Ba_2SiO_4, respectively, in order from the bottom. The inset shows the data in detail, where the arrows indicate peaks due to the supercell, which are much clear in the neutron powder diffraction pattern than in the X-ray powder diffraction pattern.

Table 1
Crystal data and structure refinement for $Ba_3MgSi_2O_8$ from combined powder X-ray and neutron diffraction data..

Chemical formula	$Ba_3MgSi_2O_8$
Formula weight	1861.341
Space group	$P\bar{3}$, (No. 147)
Z	3
a (Å)	9.72411 (3)
c (Å)	7.27647 (3)
V (Å^3)	595.870 (5)
d_{calc} (g/cm^3)	5.18710 (4)
Temperature (K)	296
Number of reflections (X-ray/neutron)	851/519
$R_p/R_{wp}/R_{exp}/R_B$ (X-ray) (%)[a]	3.15/4.07/2.94/1.25
$R_p/R_{wp}/R_{exp}/R_B$ (neutron) (%)[a]	4.50/5.92/1.76/2.02
R_p/R_{wp} (total) (%)[a]	3.78/5.02
Goodness of fit (total)	2.06
Reduced χ^2	4.20
Total refined parameters	71

[a] $R_p = 100\Sigma|Y_{o,m}-Y_{c,m}|/\Sigma|Y_{o,m}|$; $R_{wp} = 100(\Sigma w_m|Y_{o,m}-Y_{c,m}|^2/\Sigma w_m|Y_{o,m}|^2)^{1/2}$; $R_B = 100(\Sigma|I_{o,k}-I_{c,k}|/\Sigma I_{o,k})$; $\chi^2 = 100\Sigma w|I_o-I_c|^2/(N_{obs}-N_{var})$; $R_{exp} = R_{wp}/|\chi|$.

Table 2
Atomic coordinates, site occupancies and isotropic displacement (Å$^2 \times 10^2$) for $Ba_3MgSi_2O_8$ at room temperature..

Atom	Site	x	y	z	Occupancy	B_{iso} (Å^2)[a]
Ba1	1b	0	0	0.5	1	0.92 (3)
Ba2	2d	1/3	2/3	0.5037 (9)	1	0.92 (3)
Ba3	6g	0.3310 (5)	0.3302 (3)	0.8216 (1)	1	0.46 (2)
Mg1	1a	0	0	0	1	0.61 (4)
Mg2	2d	1/3	2/3	0.0081 (6)	1	0.61 (4)
Si	6g	0.3292 (8)	0.3223 (3)	0.2571 (2)	1	0.43 (4)
O1	6g	0.3500 (3)	0.3134 (2)	0.4753 (2)	1	2.15 (5)
O2	6g	0.1741 (4)	0.1777 (4)	0.1754 (7)	1	0.78 (2)
O3	6g	0.4892 (4)	0.3308 (5)	0.1586 (4)	1	0.78 (2)
O4	6g	0.3348 (4)	0.4915 (4)	0.1958 (4)	1	0.78 (2)

[a] Constraints were placed on the atomic displacement factors for Ba1 = Ba2; Mg1 = Mg2; O2 = O3 = O4.

Table 3
Selected interatomic distances (Å) and angles (degrees) in $Ba_3MgSi_2O_8$ at room temperature..

Ba1–O2 × 6	2.917 (5)	O2-Ba1-O2	61.07 (15)
Ba2–O1 × 3	2.991 (3)		180.0
–O3 × 3	2.996 (6)	O1–Ba1–O1	60.31 (6)
–O4 × 3	2.818 (6)	O1–Ba2–O1	119.74 (14)
Ba3–O1	2.538 (2)	O3–Ba2–O3	59.39 (13)
–O2	2.752 (5)	O4–Ba2–O4	63.42 (13)
–O2	2.820 (6)	O1–Ba2–O3	105.36 (14)
–O2	2.982 (6)	O1–Ba2–O4	76.33 (12)
–O3	2.800 (6)	O1–Ba3–O2	87.05 (13)
–O3	2.860 (6)	O1–Ba3–O4	155.79 (75)
–O3	2.894 (4)		80.60 (8)
–O4	2.817 (5)	Ba3–O1–Si	172.21 (9)
–O4	2.819 (6)	O2–Mg1–O2	92.08 (19)
–O4	3.134 (3)		180.00
Mg1–O2 × 6	2.135 (5)	O3–Mg2–O3	89.97 (17)
Mg2–O3 × 3	2.100 (4)	O3–Mg2–O4	85.17 (16)
–O4 × 3	2.189 (4)		92.23 (12)
Si–O1	1.608 (3)		176.67 (14)
–O2	1.577 (9)	O1–Si–O2	114.46 (22)
–O3	1.677 (6)	O1–Si–O3	106.61 (17)
–O4	1.679 (5)	O1–Si–O4	111.83 (19)
		O2–Si–O3	109.5 (3)
		O2–Si–O4	108.8 (3)
		O3–Si–O4	105.3 (4)

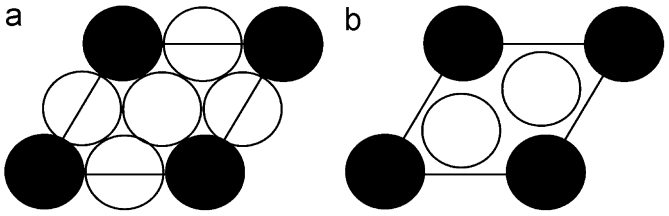

Fig. 3. Representation of hexagonal layers: (a) [AX_3] and (b) [AX_2]. A and X are cations and anions, represented by filled and open circles, respectively.

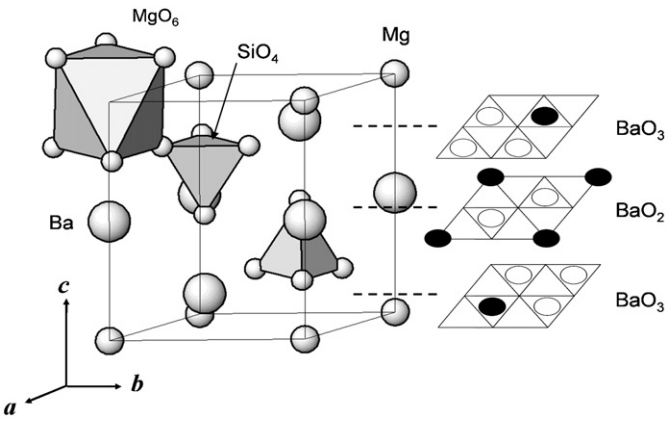

Fig. 4. The subcell crystal structure of $Ba_3MgSi_2O_8$. MgO_6 and SiO_4 are shown as an octahedron and a tetrahedron, respectively. The unit cell is outlined. Layer types are presented on the right side.

A 3-layer stacking sequence of one [BaO_2] and two [BaO_3] layers is displayed on the right side. A typical perovskite structure (ABO_3) would consist of a stacking of [AO_3] layers only. The $Ba_3MgSi_2O_8$ structure can be regarded as the replacement of every third [BaO_3] layer by a [BaO_2] layer. The Mg atoms occupy distorted octahedral sites formed by two adjacent [BaO_3] layers, as in a normal perovskite. Each [BaO_2] layer interleaved between two [BaO_3] layers creates distorted tetrahedral sites above and below the [BaO_2] layer that are occupied by the Si atoms.

3.4. Superstructure

The refined crystal structure of $Ba_3MgSi_2O_8$ is represented in Fig. 5, where the subcell–supercell relationship is also indicated. The superstructure arises from displacements of atoms Ba2, Ba3, Si, and O relative to their positions in the subcell. It should be also noted that the atoms on special positions-Ba1, Mg1, and Mg2—(cf., Table 2) remain the same. The refined Si position for the subcell was (1/3, 2/3, 0.2605) (Supporting Information), making the corresponding equivalent position in the supercell (1/3, 1/3, 0.2605). Since the refined position of Si for the supercell is (0.3292, 0.3223, 0.2571) (Table 2), the shift in position between the subcell and supercell is 0.10 Å. Similarly, such deviations were calculated for the other atoms: 0.03 (Ba2), 0.03 (Ba3), 0.31 (O1), 0.16 (O2), 0.22 (O3), and 0.19 Å (O4). On average, the Ba atoms are displaced the least, and O1 the most. Several expected superstructure peak positions are indicated as arrows in the insets in Fig. 2. Because the O atom has the smallest X-ray atomic scattering, but the strongest neutron scattering lengths, the superstructure peaks were detected only in the neutron diffraction pattern.

The crystal structure of $Ba_3MgSi_2O_8$ may also be described as a polyhedral network resulting from the corner-sharing of MgO_6 octahedra and SiO_4 tetrahedra as shown in Fig. 5; the Ba atoms

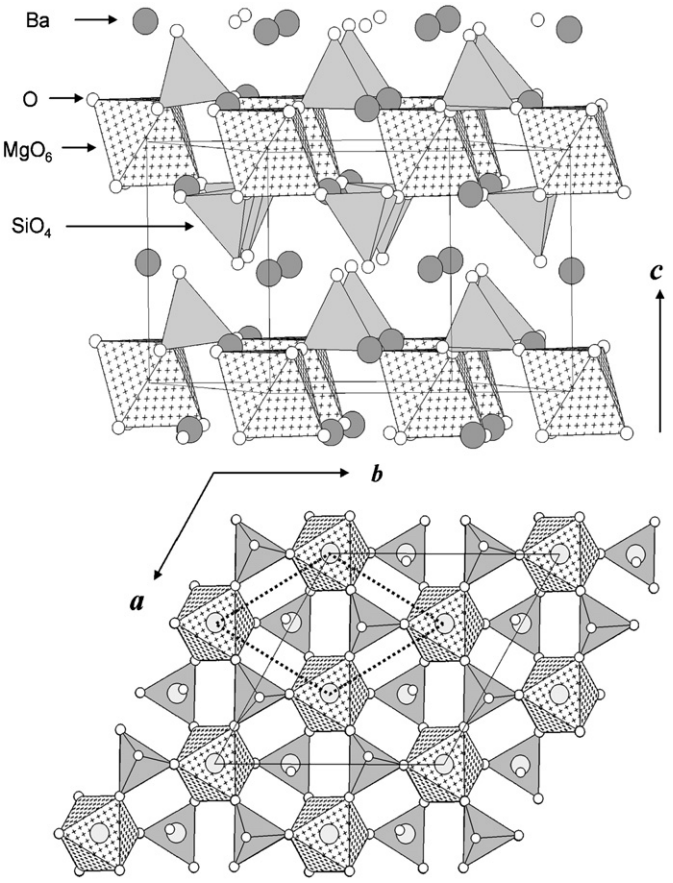

Fig. 5. Crystal structure of $Ba_3MgSi_2O_8$ viewed along the c direction (top) and projected onto the ab plane (bottom). Solid line indicates unit cell of the structure and the dotted line represents the subcell of a_o and c_o.

occupy the larger cavities surrounded by O atoms. The MgO_6 octahedron is engaged in corner-sharing with six tetrahedra, while the SiO_4 tetrahedron shares corners with three MgO_6 octahedra and the remaining apex with a Ba atom.

Three distinct local coordination environments exist for the Ba sites, as represented in Fig. 6. Ba1 occupies a distorted octahedral site with S_6 ($\bar{3}$) symmetry, surrounded by six O2 atoms at a distance of 2.917(5) Å. At a longer distance of 3.245(5) Å, six O1 atoms bind Ba1 weakly in equatorial positions. Ba2 occupies a nine-coordinate site with C_3 (3) symmetry, surrounded by three O1 atoms at a distance of 2.991(3) Å, three O3 atoms at 2.996(6) Å, and three O4 atoms at 2.818(6) Å. Ba3 occupies a 10-coordinate site with C_1 (1) symmetry, surrounded by one O1, three O2, three O3, and three O4 atoms at distances of 2.538(2)–3.134(3) Å with the average value of 2.842 Å, close to the expected d(Ba–O) value of 2.88 Å [14].

3.5. Bond-valence sums (BVS)

The empirical expression for bond valence, which has been widely adopted to estimate valences in inorganic solids, was used to check the $Ba_3MgSi_2O_8$ crystal structure. The bond valence sums [16], calculated using the software Valence [17], are 1.51 (Ba1), 1.59 (Ba2), 2.40 (Ba3), 1.82 (Mg1), 1.79 (Mg2), 3.91 (Si), 1.77 (O1), 2.29 (O2), 2.00 (O3), and 1.94 v.u. (O4). These values generally match the expected charges of the ions. The high valence sum of 2.40 for Ba3 resulted mainly from the short Ba3–O1 distance (2.538 Å). These high sums and short distances may reflect structural strain and explain the instability of $Ba_3MgSi_2O_8$ at

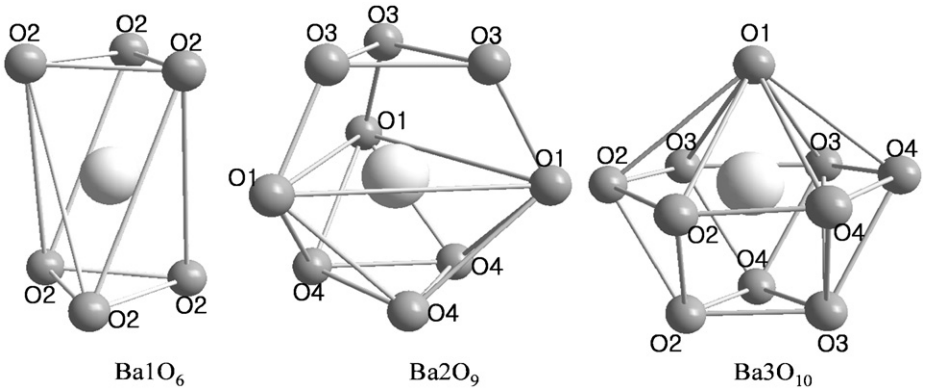

Fig. 6. The O environments about Ba1, Ba2, and Ba3 atoms.

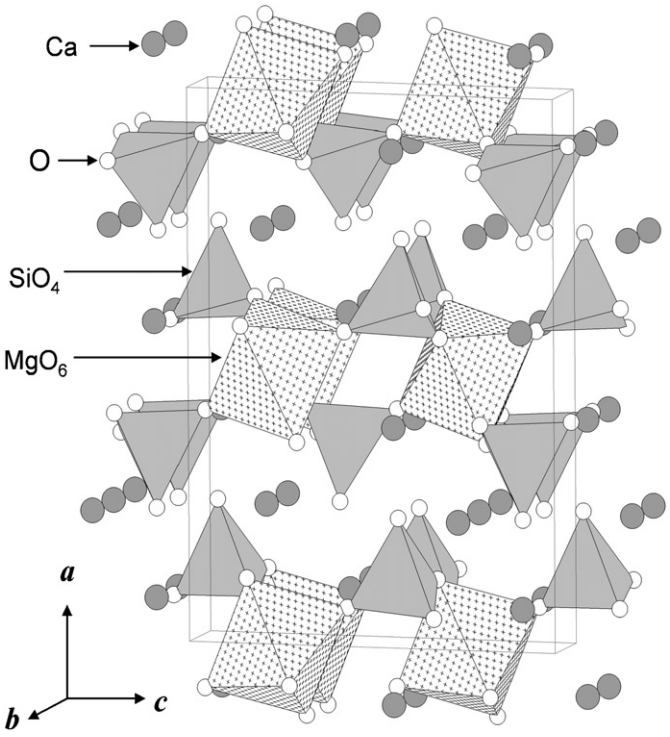

Fig. 7. The crystal structure of $Ca_3MgSi_2O_8$.

high temperatures. It is also worth noting that the calculated density (5.19 g/cm^3) of $Ba_3MgSi_2O_8$ is higher than the average density (4.75 g/cm^3) of $BaMgSiO_4$ (4.02 g/cm^3) and Ba_2SiO_4 (5.48 g/cm^3).

3.6. Comparison with related structures

Once the structure of $Ba_3MgSi_2O_8$ was solved and refined, two compounds of $K_3MP_2O_8$ (M = Sc, Lu) were found from the ICSD search with $P\bar{3}$ space group, similar unit cell dimensions, and the same atomic ratio of (3: 1: 2: 8), where K, M, and P sites correspond to Ba, Mg, and Si sites, respectively. It should be emphasized that some of the superstructure peaks for these compounds are weak but distinguishable in X-ray diffraction data, while those for $Ba_3MgSi_2O_8$ were observed only in the neutron diffraction data.

The crystal structure of $Ca_3MgSi_2O_8$ [8] is represented in Fig. 7, and the unit cell dimensions are presented in Table 4. The $Ba_3MgSi_2O_8$ structure is different from, but closely related to the

Table 4
Structural information for compounds related with $Ba_3MgSi_2O_8$..

Compound	Crystal system, space group	Unit cell	Reference
$Ba_3MgSi_2O_8$	Trigonal, $P\bar{3}$	$a = 9.72411\ (3)$ Å, $c = 7.27647\ (3)$ Å	This work
	Orthorhombic	$a = 5.5$ Å, $b = 9.8$ Å, $c = 7.6$ Å,	[7]
$K_3ScP_2O_8$	Trigonal, $P\bar{3}$	$a = 9.430\ (2)$ Å, $c = 7.629\ (2)$ Å	[18]
$K_3LuP_2O_8$	Trigonal, $P\bar{3}$	$a = 9.601\ (2)$ Å, $c = 7.725\ (4)$ Å	[19]
$Ca_3MgSi_2O_8$	Monoclinic, $P2_1/a$	$a = 13.254\ (21)$ Å, $b = 5.293\ (9)$ Å, $c = 9.328\ (17)$ Å, $\beta = 91.90\ (15)^\circ$	[8]

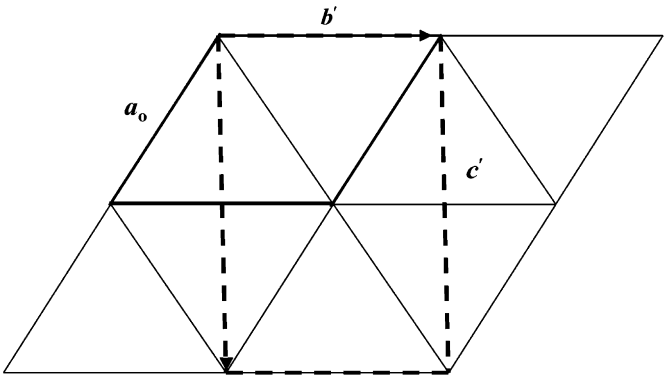

Fig. 8. Relationship between the subcell of a_o and the supercell of $a' \approx 2c_o$, $b' \approx a_o$, $c \approx \sqrt{3}a_o$, $\beta \approx 90^\circ$ for $Ca_3MgSi_2O_8$. c_o-axis is not shown for clarity.

$Ca_3MgSi_2O_8$ structure. Comparison of Figs. 5 and 7 obviously shows their similarity. It would be also very interesting to note that the crystal structure of $Ca_3MgSi_2O_8$ may be described as a supercell of its subcell with relations of $a' \approx 2c_o$, $b' \approx a_o$, $c' \approx \sqrt{3}a_o$, $\beta \approx 90^\circ$, as shown in Fig. 8. The basic structural building units are similar for the Ca and Ba compounds, but the Ca compound exhibits a stronger structural distortion than the Ba structure, leading to adoption of the lower symmetry monoclinic space group.

3.7. Structure–property relationship

Considering the three different crystallographic Ba sites in $Ba_3MgSi_2O_8$ and the sensitivity of the $4f^65d$ excited state of Eu^{2+} ion to its local environment [20], three Eu^{2+} emission bands might be expected to be observed in a luminescence spectrum. Only one emission band at 440 nm with a long tail at the longer-wavelength side, however, is observed in the room-temperature emission spectrum of Eu^{2+}:$Ba_3MgSi_2O_8$ [5]. Similarly, a single emission band at 440 nm was observed at room temperature for Eu^{2+}:$BaMgSiO_4$ [21], which also has three different Ba sites with average Ba–O distances of 2.743, 2.894 or 2.944 Å. An additional broad Eu^{2+} emission band near 560 nm has also been reported at 4.2 K for $BaMgSiO_4$ [22]. Study of temperature-dependent emission spectra indicated that the 560-nm broad band was derived from two different types of Eu^{2+} emission centers, which were quenched at room temperature [22]. Similar results might be expected for $Ba_3MgSi_2O_8$, but further study is required to assess structure-luminescence relationships of the doped host.

4. Conclusions

The crystal structure of $Ba_3MgSi_2O_8$ has been determined and refined with a combined Rietveld treatment of powder X-ray and neutron diffraction data. The neutron data were crucial to confirm and refine the $\sqrt{3} \times \sqrt{3} \times 1$ superstructure, which could not be observed from X-ray data. The superstructure was predominantly due to a small reorientation of SiO_4 tetrahedra. Interestingly, the crystal structure of $Ba_3MgSi_2O_8$ is different from, but closely related to the $Ca_3MgSi_2O_8$ structure, which may be described as $2 \times 1 \times \sqrt{3}$ type of superstructure. This work provides an important structural basis for understanding of the physical properties of an important phosphor host.

Supporting information

Table of refined atom parameters for the subcell of $Ba_3MgSi_2O_8$. X-ray Rietveld refinement profiles for $Ba_3MgSi_2O_8$, using the TOPAS software package, where the amounts of the minor impurity phases are graphically shown. Further details of the crystal structure investigations can be obtained from the Fachinformationszentrum Karlsruhe, 76344 Eggenstein-Leopoldshafen, Germany (fax: (49) 7247 808 666; e-mail: crysdata@fiz-karlsruhe.de) on quoting the depository number CSD 419862 for $Ba_3MgSi_2O_8$.

Acknowledgment

The authors would like to thank Dr. Y.N. Choi in the Korea Atomic Energy Institute, Daejeon, Korea, for assistance with the neutron powder diffraction measurement, and Mr. T.-H. Kim in LG Chem Research Park for the ICP analysis.

Appendix A. Supplementary material

Supplementary data associated with this article can be found in the online version at 10.1016/j.jssc.2008.11.024.

References

[1] J.S. Kim, A.K. Kwon, Y.H. Park, Y. Hyung, J.C. Choi, H.L. Park, G.C. Kim, J. Lumin. 122–123 (2007) 583–586.
[2] A.A. Setlur, A.M. Srivastava, H.A. Comanzo, US Patent 7026755, 2005.
[3] J.S. Kim, P.E. Jeon, J.C. Choi, H.L. Park, S.I. Mho, G.C. Kim, Appl. Phys. Lett. 84 (15) (2004) 2931–2933.
[4] J.S. Kim, J.Y. Kang, P.E. Jeon, J.C. Chol, H.L. Park, T.W. Kim, Jpn. J. Appl. Phys. 43 (2004) 989–992.
[5] S. Kamiya, H. Mizuno, in: S. Shionoya, W.M. Yen (Eds.), Phosphor Handbook, CRC Press, Boca Raton, 2000, pp. 414–415.
[6] T.L. Barry, J. Electrochem. Soc. 115 (7) (1968) 733–738.
[7] H.A. Klasens, A.H. Hoekstra, A.P.M. Cox, J. Electrochem. Soc. 104 (2) (1957) 93–100.
[8] P.B. Moore, T. Araki, Am. Miner. 57 (1972) 1355–1374.
[9] H.P. Grosse, E. Tillmanns, Cryst. Struct. Commun. 3 (1974) 599–601.
[10] B. Liu, J. Barbier, J. Solid State Chem. 102 (1993) 115–125.
[11] R.W. Cheary, A. Coelho, J. Appl. Crystallogr. 25 (1992) 109–121 Bruker AXS, TOPAS 3, Karlsruhe, Germany, 2000.
[12] P.E. Werner, L. Eriksson, M. Westdahl, J. Appl. Crystallogr. 18 (1985) 367–370.
[13] ICSD (Inorganic Crystal Structure Database), version 2005-1, Karlsruhe, Germany.
[14] R.D. Shannon, Acta Crystallogr. A 32 (1976) 751–767.
[15] J. Darriet, M.A. Subramanian, J. Mater. Chem. 5 (4) (1995) 543–552.
[16] I.D. Brown, D. Altermatt, Acta Crystallogr. B 41 (1985) 244–247.
[17] N.E. Brese, M. O'Keeffe, Acta Crystallogr. B 47 (1991) 192–197.
[18] V.A. Efremov, P.P. Mel'nikov, L.N. Komissarova, Revue de Chimie Minerale 22 (1985) 666–675 ICSD #61786.
[19] V.A. Efremov, P.P. Mel'nikov, L.N. Komissarova, Phase Transition 38 (1992) 127–220 ICSD #66876.
[20] G. Blasse, B.C. Grabmaier, Luminescent Materials, Springer, Berlin, 1994.
[21] G. Blasse, W.L. Wanmaker, J.W. Ter Vrugt, A. Bril, Philips Res. Rep. 23 (1968) 189–200.
[22] S.H.M. Poort, H.M. Reijnhoudt, H.O.T. Van der Kuip, G. Blasse, J. Alloys Compd. 241 (1996) 75–81.